## scientific reports



### OPEN

# Structural and dynamic basis of Ssp4-mediated DNA protection in foodborne bacterial spores

Minseok Seo<sup>1</sup>, Bokyung Kim<sup>1</sup>, Hyogyung Shin<sup>1</sup>, Jinwoo Kim<sup>1</sup>, Jong-Bong Lee<sup>2</sup>, Young Ho Ko<sup>3</sup>, Jin Hae Kim<sup>1</sup> & Yoori Kim<sup>1⊠</sup>

Clostridium perfringens forms metabolically dormant endospores that withstand extreme environmental conditions. Small acid-soluble proteins (SASPs) are ubiquitous DNA-binding proteins in endospores that promote resistance. While their protective role has been previously characterized, we aimed to provide further biophysical insight into the nature of these interactions, focusing on variant-specific structural dynamics through novel single-molecule and NMR approaches. Here, we characterize the DNA-binding properties and structural features of two Ssp4 variants using single-molecule fluorescence imaging and NMR spectroscopy along with electrophoretic mobility shift assays (EMSA). Both Ssp4 variants bind DNA cooperatively, but single-molecule analysis revealed preferential binding to GC-rich regions and significantly increased residence time in the presence of dipicolinic acid (DPA). NMR analysis reveals that an aspartic acid residue at position 36 (D36) stabilizes the Ssp4 structure, and its removal induces local structural perturbations without altering DNA affinity. Our findings provide molecular insights into how Ssp4 variants protect DNA in substantially dehydrated endospores and promote spore survival.

Clostridium perfringens is a spore-forming bacterium that causes gas gangrene, botulism, and food poisoning  $^{1-4}$ . Its ability to form metabolically dormant endospores enables survival under extreme environmental stresses such as heat, desiccation, and UV irradiation (Fig. S1) $^{5.6}$ . These spores are  $\sim 1~\mu m$  in length and contain a core with low water content ( $\sim 20\%$  of wet weight), which houses a complete copy of the bacterial genome  $^{7.8}$ . The genomic DNA is highly compacted and must be effectively protected until conditions become favorable for germination  $^{6.9,10}$ . During the sporulation, *C. perfringens* synthesizes a variety of endospore-specific proteins that contribute to spore maturation and environmental resistance. Among these, small acid-soluble proteins (SASPs) are highly conserved, abundant DNA-binding proteins that are rapidly produced during sporulation and degraded upon germination (Fig. 1A) $^{11-14}$ . Previous studies demonstrated that reducing SASPs by antisense RNA or null mutant leads to decreased spore resistance against heat, low temperature, UV irradiation, and nitrous acid<sup>13,15</sup>.

Among the four types of *C. perfringens* SASPs (Ssp1 – Ssp4), Ssp4 has been identified as an important factor contributing to spore resistance through its ability to bind DNA $^{16}$ . Particularly, strains that produce the Ssp4 variant with an aspartic acid at position 36 (Ssp4 $_{D36}$ ), which is frequently found in food-poisoning isolates, exhibit significantly higher heat resistance than those carrying glycine at the same residue (Ssp4 $_{G36}$ ) (Fig. 1B) $^{16,17}$ . This correlation between amino acid variation and phenotypic resistance suggests a structural and functional specificity of Ssp4, possibly linked to its interaction with genomic DNA. Nevertheless, how such sequence variants modulate DNA binding and influence spore robustness remains poorly defined.

In this study, we aim to elucidate the molecular interaction by which Ssp4 contributes to genome protection and spore resistance in *C. perfringens*. Using a combination of electrophoretic mobility shift assays (EMSAs), single-molecule fluorescence imaging, and nuclear magnetic resonance (NMR) spectroscopy, we analyze the DNA-binding dynamics of Ssp4 variants and its structural characteristics. Our findings reveal that Ssp4 preferentially binds GC-rich DNA sequences in a cooperative manner and this interaction is modulated by specific residue variations. These insights provide a mechanistic framework for understanding how SASPs, particularly Ssp4, safeguard the genome in dormant spores and contribute to the pathogen's environmental resilience.

<sup>1</sup>Department of New Biology, New Biology Research Center, Daegu Gyeongbuk Institute of Science and Technology (DGIST), Daegu 42988, Republic of Korea. <sup>2</sup>Department of Physics, Division of Interdisciplinary Bioscience and Bioengineering, Pohang University of Science & Technology (POSTECH), Pohang 37673, Republic of Korea. <sup>3</sup>Center for Epitaxial van der Waals Quantum Solids, Institute for Basic Science, Pohang 37673, Republic of Korea. <sup>™</sup>email: yoori.kim@dgist.ac.kr

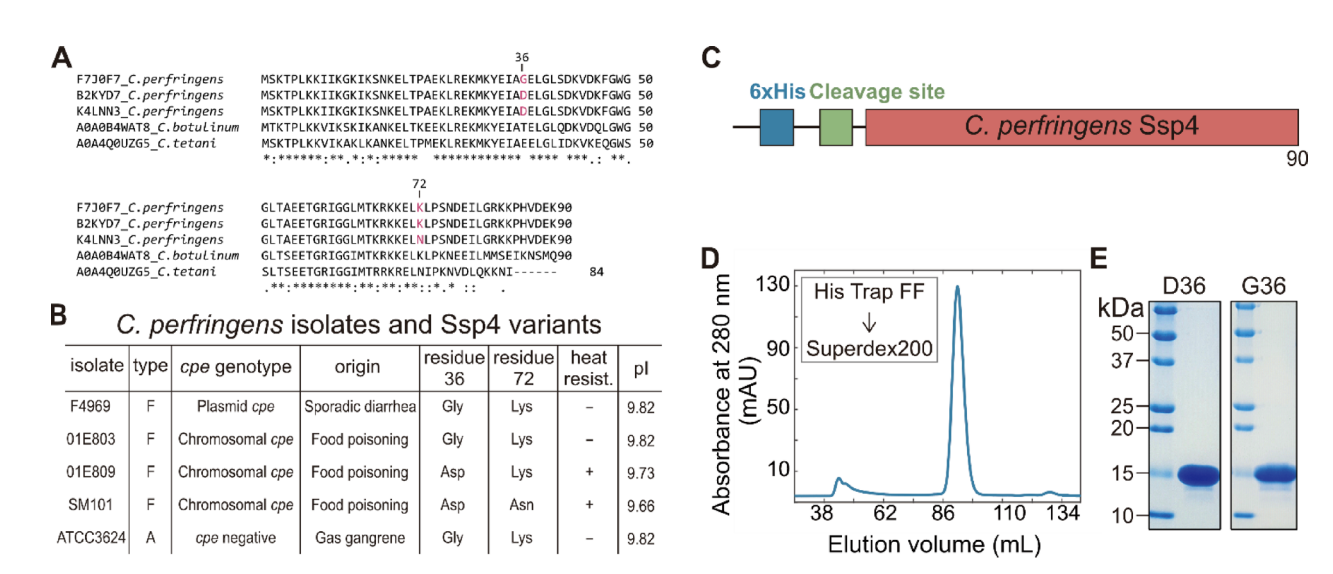


**Fig. 1.** SASP homology, the features and purification of Ssp4 variants. (**A**) Multiple sequence alignment of Ssp4 with other SASPs from various *Clostridium* species. Magenta residue indicates variant residues in Ssp4. (\*) fully conserved residue; (:) conservative mutation; (.) semi-conservative mutation. (**B**) The features of *C. perfringens* Ssp4 variants <sup>16,47,48</sup>. (**C**) The domain structure of Ssp4. The vector produced a His-tagged Ssp4 with a thrombin cleavage site between the His-tag and *ssp4* gene (~ 12.3 kDa). (**D**) The elution profile of HiLoad 16/600 superdex 200 pg after HisTrap FF crude column to capture the proteins with His-tagged. (**E**) Coomassie blue-stained 15% SDS-PAGE gel showing a selected region of the HisTrap FF elution samples of Ssp4<sub>D36</sub> and Ssp4<sub>G36</sub>, collected prior to the size-exclusion chromatography. The full gel image showing all purification steps is provided in (Supplementary Figure S2).

#### Results

#### Characterization of Ssp4 DNA binding properties and cooperative interaction

To characterize the DNA binding properties and its associated functional mechanism of the Ssp4, we expressed recombinant Ssp4 variants (Ssp4 $_{D36}$  and Ssp4 $_{G36}$ ) with an N-terminal 6xHis tag and purified them (Fig. 1C). Both proteins were purified to high purity and yield using nickel affinity and size exclusion chromatography (Fig. 1D–E, Fig. S2). As a starting point for our subsequent biophysical analyses, we initially performed gel-based biochemical assays informed by previous studies on SASP-DNA interactions <sup>18–20</sup>. We first conducted EMSA with 100–300 bp DNA containing half of GC content on average. As the ratio of Ssp4 to DNA concentration increases, the fraction of free DNA decreased by the shifted DNA–Ssp4 complex formation (Fig. 2A). When the molar ratio of Ssp4 to DNA reached 120:1, more than 90% of DNA was occupied by the proteins.

To quantitatively compare the DNA binding affinity and assess cooperative binding, the half-saturation constants ( $K_{0.5}$ ) were calculated by fitting the Hill equation in various conditions (Fig. 2B).

2D). The extracted  $K_{0.5}$  values of Ssp4 with the DNA used were 737  $\pm$  10.6 nM on average. There was no significant difference in  $K_{0.5}$  either between the two variants across all tested DNA substrates, or between DNA substrates of different sizes (Fig. 2C). Furthermore, we tested the Hill slope (h) values to evaluate cooperative binding to DNA, which appeared to be above four as positive values regardless of DNA size or variant type (Fig. 2D). Despite no observable difference between DNA sizes, the Hill slope of Ssp4<sub>D36</sub> was significantly larger than that of Ssp4<sub>G36</sub> in 100 bp DNA, implying that the DNA binding mode with positive cooperativity might become evident in shorter DNA or locally in the case of Asp variant. Although His-tags may influence protein–DNA interactions, previous studies have shown that they do not significantly affect DNA binding affinity<sup>21,22</sup>. To verify this in our system, we conducted EMSA using Ssp4 variants lacking the His-tag and observed comparable DNA binding affinity, suggesting that the His-tag does not substantially alter the DNA binding properties of Ssp4 (Fig. S3).

UV irradiation is a widely used sterilization method by damaging bacterial DNA. To test whether the DNA-binding activity of the Ssp4 variants contributes to the protection against UV-induced DNA damage, we first observed the effect of UV-A on DNA by EMSA. The UV-induced damage rendered the DNA smear and moved slowly compared to the intact DNA, and the degree of the DNA migration decreased as a function of time exposed to UV (Fig. S4A). This result is consistent with a previous AFM result which demonstrated that the UV-exposed DNA displays kinked, knot-like structures and thereby becomes compacted overall<sup>23</sup>. The UV-induced alteration of DNA mobility was alleviated upon Ssp4 binding (Fig. S4B). For quantitative analysis, each vertical distribution of DNA intensity on the gel was represented by plotting a curve. In the presence of UV irradiation, the peak of the curve representing the Ssp4-bound DNA was closer to the intact DNA compared to the absence of protein-bound, suggesting the role of Ssp4 in DNA protection against UV-induced structural alteration (Fig. S4C). No significant difference was found between the two Ssp4 variants in the UV-mediated gel shift measurements. To further test the physical protective effect of Ssp4 binding on DNA, DNase I was treated with

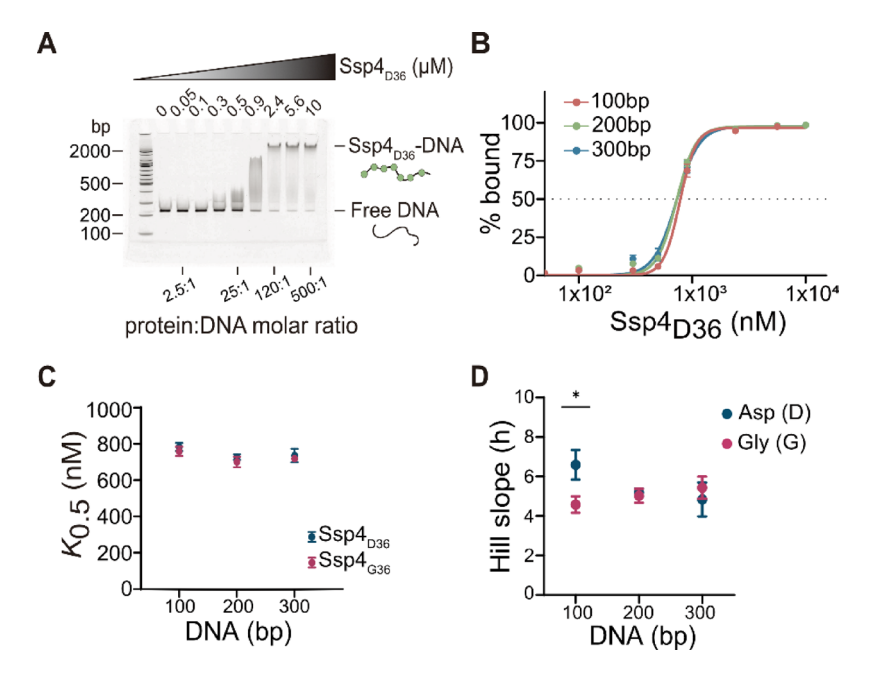


**Fig. 2.** Quantitative characterization of DNA interaction activity of Ssp4 variants. (**A**) 6% native-PAGE gel depicting the binding between 200 bp DNA and Ssp4<sub>D36</sub>, with increasing Ssp4 concentrations ranging from 0.05 to 10 μM. The DNA concentration is maintained at 20 nM. (**B**) Fitted curves with a logarithmic scale X-axis illustrating DNA binding affinity for Ssp4<sub>D36</sub>. Comparison of the half-saturation constant ( $K_{0.5}$ ) (**C**) and Hill coefficients (h) (**D**) depending on DNA length for both Ssp4<sub>D36</sub> and Ssp4<sub>G36</sub> variants.

varying concentrations of Ssp4. The enzyme considerably digested the DNA tested by itself whereas the portion of intact DNA molecules increased as a function of Ssp4 concentration (Fig. S4D–F). Although the degree of DNA protection was comparable between Ssp4 $_{\rm G36}$  and Ssp4 $_{\rm D36}$  for both 100 bp and 300 bp substrates, the protection level significantly increased as the protein occupancy reached high binding levels (> 70%), at which a substantial fraction of DNA was protected, whereas the enzyme almost completely degraded DNA at low Ssp4 binding ( $\leq$  10%) (Fig. S4E–F). Given that enzyme activities are limited in the low-hydration endospore, even slightly increased DNA protection level could be a significant defense on the compact spore DNA damage patterns by promoting the formation of the spore photoproduct (SP), a unique thymine dimer typically associated with spores, while reducing the formation of canonical thymine dimers such as cyclobutane pyrimidine dimers and pyrimidine (6 – 4) pyrimidone dimers  $^{19,24}$ . Although SP formation occurs independently of DPA, DPA may still influence UV-induced DNA photochemistry as a potential photosensitizer  $^{24,25}$ . Consistent with this protective mechanism, our observation that Ssp4 binding enhances resistance to enzymatic degradation further supports the protective role of SASP-DNA interactions in preserving spore DNA integrity under stress conditions.

#### Single-molecule study of Ssp4-DNA interaction

To further examine the DNA binding dynamics for the Ssp4 variants, we used total internal reflection fluorescence microscopy (TIRFM) to directly observe protein behavior in real-time on the arrays of single DNA molecules supported on a lipid bilayer (Fig. 3A) $^{26,27}$ . Because SASPs are relatively small peptides reaching at most  $\sim 10$  kDa, using a large antibody ( $\sim 150$  kDa) for an in vitro immunofluorescence can hinder the binding dynamics of the protein on DNA. Thus, we adapted a sortase-mediated labeling reaction to directly conjugate the Atto488 fluorophore into the protein with minor modification $^{28}$ . The fluorescently labeled Atto488-Ssp4 rapidly bound to the DNA arrays as soon as it entered the flowcell. Interestingly, the immediate DNA binding of Ssp4 covered the whole DNA except for the GC-poor region in the middle (Fig. 3B). The preferential binding for GC-rich sequences was prominent on the DNA arrays, with a consistent pattern observed for both Gly and Asp variants (Fig. 3C). The correlation analysis for the binding distribution between Ssp4 $_{\rm G36}$  and Ssp4 $_{\rm D36}$  showed a high correlation coefficient in the linear fitting (slope = 1.1,  $\rm R^2 = 0.93$ ), indicating that there is no statistical difference in the preferential binding for GC sequences (Fig. 3D). Although the GC content of the *C. perfringens* genome has been reported to be relatively low at 28.6%, local GC-rich regions scattered throughout the genome may contribute to the preferential binding and protecting the DNA $^{29}$ .

A key feature of bacterial endospores is the low water content of their core. This condition is initially driven by cortex and coat assembly, which compress the core and reduce its water content. DPA and calcium ions (Ca<sup>2+</sup>) are then taken up, replacing residual water and further lowering the hydration level<sup>10,30,31</sup>. To test the impact of DPA on the dynamic behavior of SASPs on DNA, we analyzed the relative residence time (or dwelling time) on DNA in the presence and absence of DPA using single-molecule imaging. Because the individual DNA binding of fluorescent Ssp4 was too dense to count, we quantified the relative half-life of the protein on DNA by fitting an exponential decay curve to the fluorescent intensity profiles acquired from consecutive images (Fig. S5A).

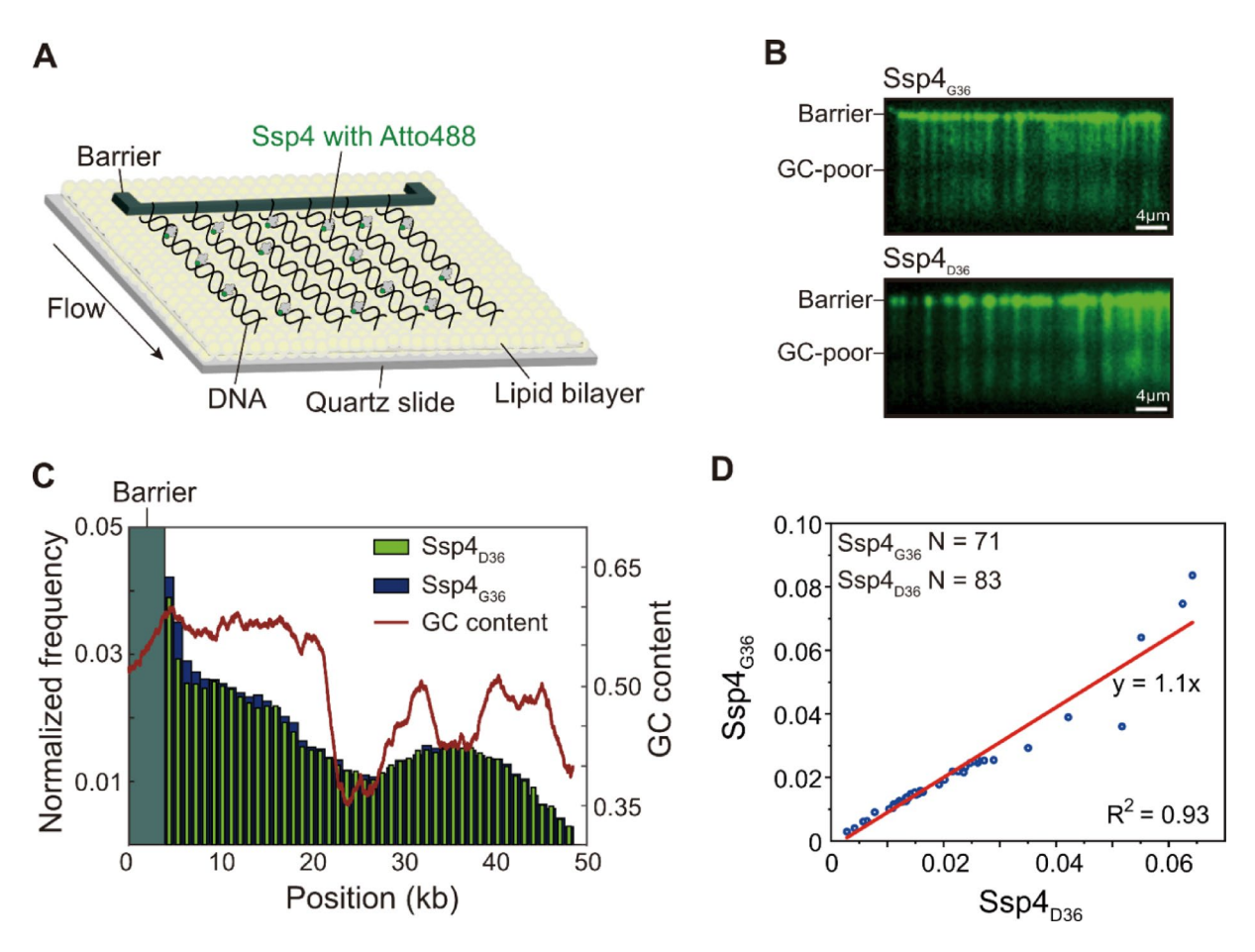


**Fig. 3.** Direct visualization of Ssp4 variants by Single-molecule DNA curtain assays. (**A**) Schematic of the DNA curtains assay with Ssp4. The flowcell surface is passivated with a lipid bilayer. DNA is affixed to the lipid bilayer, organized at nano-fabricated barriers. (**B**) DNA curtain with fluorescent Ssp4 (Green) variants (Ssp4 $_{G36}$  top or Ssp4 $_{D36}$  bottom) in the presence of buffer flow. (**C**) Ssp4 protein binding distribution on λ-DNA (n=83 for Ssp4 $_{D36}$ , n=71 for Ssp4 $_{G36}$ ). The probability of GC content in λ-DNA is shown as a red line. The distribution of Ssp4 on DNA curtain demonstrates preference for GC-rich DNA regions relative to AT-rich sequences. (D) Correlation between the binding frequency of Ssp4 $_{G36}$  and Ssp4 $_{D36}$  on DNA. The linear fit to data yields a slope of  $m=1.10\pm0.04$  ( $R^2=0.93$ ), indicating no statistical difference in the binding preference between Ssp4 $_{G36}$  and Ssp4 $_{D36}$ .

Because of the continuous buffer flow applied to stretch DNA molecules, the possibility of re-binding after dissociation could be excluded and allow to observe dissociating dynamics in real-time. Our single-molecule analysis has shown that the median half-life of each Ssp4 variant in the absence of DPA is 17.6 s (Gly) and 20.6 s (Asp), suggesting that Ssp4<sub>D36</sub> molecules were bound slightly longer compared to Ssp4<sub>G36</sub> (Fig. S5B). Interestingly, the half-life of both variants increased upon the addition of 100 nM DPA, with the half-life of Ssp4<sub>D36</sub> approximately doubling under this condition (Fig. S5B). Although this DPA concentration is orders of magnitude lower than the very high millimolar (mM) Ca-DPA concentrations found in the spore core, where DPA can constitute up to 5–15% of the dry weight and exists largely in a solid-like state, it was chosen to allow detection of potential modulatory effects on Ssp4-DNA interactions in vitro, as preliminary indicated that higher DPA concentrations had little to no additional impact on DNA binding<sup>32</sup>. These single-molecule data suggest that DPA can modulate the stability of Ssp4-DNA interactions under in vitro conditions. This finding implies that Ca-DPA may contribute to stabilizing the protective association between SASPs and spore DNA. We speculate that the increased dwelling time of such DNA-protective proteins contributes to the high resistance of DPA-replete spores to heat and chemical stress<sup>10,17</sup>.

#### NMR characterization for structural dynamics of Ssp4

Although no experimental structure of Ssp4 has been reported to date, two noteworthy models provide relevant information about the structural state of Ssp4. The first model could be obtained from the AlphaFold database (Fig. 4A)<sup>33</sup>. This model predicts that Ssp4 consists of five  $\alpha$ -helices (henceforth denoted to  $\alpha$ 1 thru  $\alpha$ 5), of which three helices ( $\alpha$ 2- $\alpha$ 4) were shown with high confidence. Furthermore, the AlphaFold model suggests that D36 is located at the terminal of  $\alpha$ 2, and its carboxylic acid side chain forms a hydrogen bond with the hydroxyl group of S41 located at  $\alpha$ 3. The second model was constructed by the Alphafold3 modeling structure of the

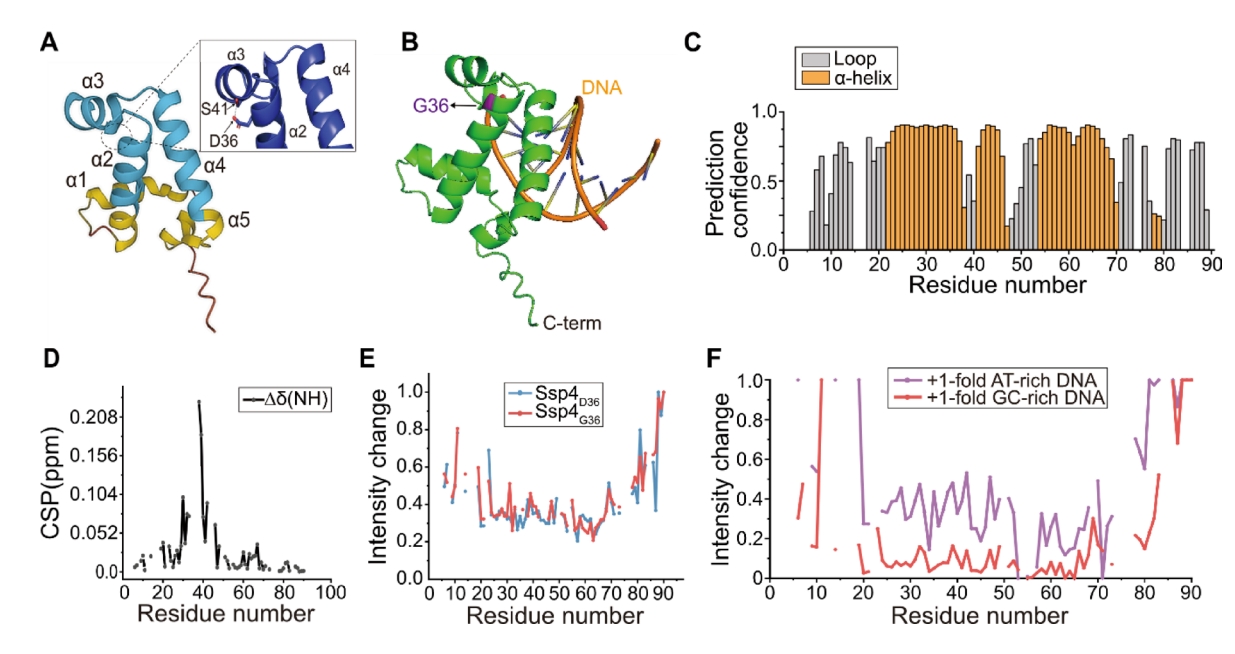


**Fig. 4.** The NMR analysis for structural insights and functional implication of Ssp4 variants. (**A**) The AlphaFold model of Ssp4 (AF-F7J0F7-F1). This model shows that Ssp4 may have five α-helices: L6-K15 (α1), P22-E37 (α2), S41-F47 (α3), A54-E70 (α4), and N76-I79 (α5). The model was colored according to the prediction confidence of each residue: (blue) higher than 70, (yellow) between 50 and 70, (orange) less than 50. The AlphaFold model of Ssp4<sub>D36</sub> predicted the hydrogen bond between the sidechains of D36 and S41. This may contribute to the stabilization of the interactions between α2 and α3/α4. (**B**) The AlphaFold3 model of *C. perfringens* Ssp4 with a 10 bp DNA (5'-CCGACGTTG-3'). Ssp4 with G36 was shown in purple, the DNA backbone was shown in orange. Residue 72 was not shown in this data. (**C**) The secondary structure prediction result obtained by TALOS-N from the assigned chemical shift information. The residues were colored according to their prediction results (green, α-helix; grey, disordered loop) along with prediction confidence on the y-axis. The signals for the residues M1–T4, K15–N17, P74–S75, and K84–P85 could not be assigned, thus not being included to prediction. (**D**) The chemical shift perturbation (CSP) by substitution of D36 with G36. (**E**) Relative intensity changes of Ssp4 signals upon addition of 0.2x dsDNA (GC-rich). (**F**) The relative signal intensity change of Ssp4<sub>D36</sub> by addition of 1-equivalent AT-rich DNA (purple) was compared with the result obtained in the presence of 1-equivalent GC-rich DNA (red).

DNA bound Ssp4 from *C. perfringens* (Fig. 4B). Notably, the  $\alpha$ -helical structures around the  $\alpha 2$  and  $\alpha 4$  regions of the AlphaFold model were also seen in the X-ray model of SspC from *Bacillus subtilis* (PDB 2z3x), predicting that Ssp4 could use this region for DNA binding<sup>34</sup>. To test whether this AlphaFold prediction is relevant in the actual experimental condition, we collected and analyzed 2D and 3D NMR spectra of Ssp4<sub>D36</sub> uniformly labeled with<sup>13</sup>C and<sup>15</sup>N, which resulted in the successful assignment of  $\sim 85\%$  backbone<sup>1</sup>–<sup>15</sup> N signals. To assess the propensity of Ssp4 for forming an  $\alpha$ -helix or a  $\beta$ -strand, we employed TALOS-N, which predicts secondary structures based on chemical shift data (Fig. 4C)<sup>35,36</sup>. This result indicates that the residues P22–E37, S41–K46, and A54–K69 have high probability to form  $\alpha$ -helices, which is consistent with the AlphaFold prediction assigning  $\alpha$ -helical elements at the residues L6–K15 ( $\alpha$ 1), P22–E37 ( $\alpha$ 2), S41–F47 ( $\alpha$ 3), A54–E70 ( $\alpha$ 4), and N76–I79 ( $\alpha$ 5). Considering low prediction confidence for  $\alpha$ 1 and  $\alpha$ 5, our NMR data proved that the AlphaFold model sufficiently represents the actual structural state of Ssp4 in a physiological condition.

To evaluate the effect of the D to G substitution of the residue 36 in Ssp4, we analyzed the NMR spectra of Ssp4 $_{G36}$  and compared it with that of Ssp4 $_{D36}$  (Fig. S6). As expected, the signal perturbation was the most severe around the substitution site (Fig. 4D). However, the residues at  $\alpha 3$  (S41-K46) also exhibited significant signal perturbations despite their distal location from D36 at the primary structure. This indicates that the D to G substitution may incur structural changes on  $\alpha 3$  and  $\alpha 2$ . Subsequently, we conducted DNA titration experiments with GC-rich duplex DNA for the Ssp4 variants to evaluate the effect of the amino acid substitution on the DNA binding dynamics (Fig. 4E and Fig. S7–S8). Notably, the signal intensity for the residues E24-I71 exhibited a simultaneous decrease in both variants, indicating that the regions  $\alpha 2-\alpha 4$  may behave as one unit to interact with DNA (Fig. 4E). However, the analyzed CSP and signal intensity change were comparable with one another, suggesting that the substitution of D36 to G36 does not exert significant effect on the DNA interaction of Ssp4, which is in accord with our EMSA result (Fig. 4D–E). Finally, to verify the preferential interaction of Ssp4 $_{D36}$  to GC-rich DNA, we repeated the same titration experiments with AT-rich DNA. Indeed, the addition of 1-equivalent GC-rich DNA to Ssp4 $_{D36}$  incurred a nearly complete disappearance of the Ssp4 signals, while the same amount of AT-rich DNA caused only a ~ 60% decrease in signal intensity, substantiating the preference for GC sequences of the protein (Fig. 4F).

#### Discussion

In this study, we investigated the molecular basis by which Ssp4 contributes to spore resistance in *C. perfringens*. Using complementary biophysical and structural approaches, identify Ssp4 as a critical DNA binding protein that safeguards the genome through dynamic and cooperative interactions. Our results provide new mechanistic insights by clarifying a reproducible preference of GC-rich DNA, the ability of DPA-Ca<sup>2+</sup> to prolong the duration of Ssp4 binding on DNA, and the effect of a single amino acid substitution at residue 36 on protein stability.

Our results indicate that Ssp4 exhibits a modest but reproducible preference for GC-rich DNA sequences, as shown by both single-molecule imaging and EMSA assays (data not shown). This observation differs from the earlier EMSA report by Li et al., which suggested preferential binding to AT-rich DNA, but aligns with the general model proposed by Setlow that SASPs preferentially interact with GC-rich regions due to their propensity to form A-like DNA structures under conditions of low water content<sup>20,37</sup>. The study by Li et al. therefore represented a potential exception in the specificity of SASPs<sup>17,37</sup>.

We consider two factors that may account for the differences between our findings and the previous EMSA results. First, methodological variations in protein purification could have influenced the observed binding specificity. While the earlier study employed only Ni-NTA affinity chromatography, we incorporated additional purification steps, including salt condition optimization and size-exclusion chromatography, to obtain highly homogeneous Ssp4 preparations (Fig. S2). Second, the nature of the assays themselves may account for the contrasting outcomes. EMSA measures equilibrium binding, in which proteins can repeatedly bind and dissociate until stable complexes are formed, potentially masking transient interactions. In contrast, single-molecule imaging captures individual binding and dissociation events in real-time, revealing short-lived GC-preferential interactions that may not be detected in bulk assays (Fig. 3B-C). Together, these complementary perspectives underscore the importance of considering both protein purity and assay methodology when evaluating the DNA-binding specificity of SASPs. Nevertheless, further studies will be required to determine whether GC preference is a general feature of SASPs.

The fact that the *C. perfringens* genome is overall AT-rich raises the question of how protection is efficiently achieved across such regions<sup>29</sup>. One possibility is that diverse DNA-binding proteins, including multiple SASPs, act collaboratively to ensure broad sequence coverage and comprehensive protection of the entire genome<sup>17</sup>. Another possibility is that DNA repair pathways compensate for sequence-specific binding biases of SASPs. In particular, spore photoproduct (SP) lyase specifically repairs thymine-derived lesions, which predominantly occur in AT-rich regions, potentially offsetting reduced SASP occupancy at these sites<sup>38,39</sup>. Taken together, these considerations suggest that both sequence-specific binding of SASPs and specialized DNA repair mechanisms act in concert to provide robust protection of the AT-rich genome in dormant spores.

One of the major features of bacterial spores is the high concentration of DPA– $Ca^{2+}$  in the core, which contributes to the loss of water content and inhibits protein mobility and enzymatic activity  $^{10,40}$ . Our single-molecule results suggest that the presence of DPA can increase the DNA residence time of Ssp4, particularly in the D36 variant (Fig. S5). We tested the DPA effect on Ssp4–DNA binding using conventional EMSA by titrating DPA– $Ca^{2+}$  concentrations up to 5 $\mu$ M, but DNA binding was largely unaffected or slightly reduced at higher concentrations under the conditions tested (data not shown). This suggest that the steady-state binding affinity of Ssp4 on DNA is not measurably altered by DPA– $Ca^{2+}$  under equilibrium conditions. The increased residence time observed in the presence of DPA at the single-molecule level suggests that DPA may modulate the kinetic stability of the Ssp4–DNA complex, potentially by influencing the local hydration state or electrostatic environment  $^{8,40}$ . These results indicate that DPA enhances DNA protection not by increasing binding affinity, but by prolonging the duration of individual protein–DNA interactions, an effect that is critical within the core but may be masked in bulk ensemble assays.

Previous research suggests that GC-rich DNA can adopt A-form DNA that is stable under low humidity<sup>41–43</sup>. Given that the accumulation of DPA-Ca<sup>2+</sup> further lowers the water content of the spore core, we initially hypothesized that this low-hydration environment would promote the transition of DNA to the A-form, thereby enhancing the binding of spore-specific proteins that protect DNA<sup>37</sup>. However, our CD spectrometry results showed that even with the addition of 10 µM DPA-Ca<sup>2+</sup>, the DNA structure remained in its stable B-form under our experimental conditions, suggesting that DPA-Ca<sup>2+</sup> does not induce structural changes in DNA (Fig. S9). This suggests that while DPA-Ca<sup>2+</sup> slightly enhances the initial Ssp4–DNA interaction, this effect does not arise from inducing structural changes in the DNA itself but may result from stabilizing effect of DPA-Ca<sup>2+</sup> on the Ssp4 protein.

We found that the DPA effect on elevated residence time of Ssp4 on DNA has been even more substantial in the case of the D36 variant, which could account for the mechanism by which the two food poisoning isolates display different spore sensitivity to heat (Fig. 1B)<sup>16</sup>. We thus explored the structural difference between  $\mathrm{Ssp4}_{\mathrm{G36}}$  and  $\mathrm{Ssp4}_{\mathrm{D36}}$ , initially by predicting the DNA interaction for  $\mathrm{Ssp4}$  using Pymol software. To assist in this prediction, we first analyzed the structure of SspC from Bacillus subtillis bound to a 10 bp DNA structure (Fig. S10)<sup>34</sup>. Since SspC is a DNA-binding protein and shares structural and functional similarities with Ssp4, it served as a useful reference for our predictive model. It is consistent with our observation that the variations at residue 36 did not directly contact the DNA. Our NMR analysis verified that the AlphaFold model of Ssp4, particularly in the  $\alpha 2$ - $\alpha 4$  region where prediction confidence was high, provides valid and useful information to evaluate the structural and functional features of Ssp4. According to the AlphaFold model, D36 is located at the tip of α2, and its carboxylic acid side chain forms a hydrogen bond with the hydroxyl group of S41, which is located at α3. This observation implies that the replacement of this residue with glycine may (1) weaken the interaction between α2 and α3, and (2) compromise the overall stability of α2 due to the intrinsic flexibility of a glycine. Our NMR analysis provided consistent evidence in which the signals for the residues at α3 were significantly perturbed by the substitution of D36 to G36. The NMR titration experiments also demonstrated that this amino acid change does not affect the binding interaction of Ssp4 for GC-rich duplex DNA. This result corroborates that D36 does not directly participate in the binding interaction with DNA. Still, our NMR results, as well as the AlphaFold model, suggest that the substitution of D36 may weaken the interaction of  $\alpha$ 2 with  $\alpha$ 3/ $\alpha$ 4, whose manifestation may be visible only in harsh conditions.

The NMR titration experiments with AT-rich and GC-rich DNA duplexes showed that the interaction of  $Ssp4_{D36}$  for GC-rich DNA is stronger than that for AT-rich DNA. The NMR signal perturbation results indicated that the region  $\alpha 2$ - $\alpha 4$  may behave as one unit to interact with DNA, while the contribution from the other regions could be less significant. Still, it was notable that some signals, such as the ones corresponding to the residues I9, L80, and V87, showed significant intensity change, and other signals corresponding to the N- and C-terminal regions exhibited noticeable movements during the titration, implying that additional contribution from the regions out of  $\alpha 2$ - $\alpha 4$  cannot be excluded fully. In addition, NMR signals of  $Ssp4_{D36}$  were mostly broadened even in the presence of 0.4-equivalent of GC-rich DNA, suggesting that more than one molecule of Ssp4 could bind to each DNA molecule, which our EMSA result has suggested. A similar binding was previously observed in the X-ray crystallographic model for *B. subtilis* SspC, in which three molecules of SspC bound to one 10 bp DNA duplex<sup>34</sup>. Further studies are necessary to validate the stoichiometry of this interaction.

In conclusion, we enhanced our understanding of the molecular basis by which SASP-DNA interactions promote DNA protection and spore resistance, and further showed that even a single amino acid residue substitution can alter this interaction, ultimately influencing spore resistance. Indeed, the DNA-protective function of Ssp4 is not limited to foodborne isolates but is a general feature of *C. perfringens* spores. Similar mechanisms may be present in other spore-forming pathogens<sup>44,45</sup>. The established strategy for fluorescent labeling of SASPs, combined with detailed structural characterization, provides a valuable platform for future investigations. This approach can facilitate studies of distinct DNA-binding modes exhibited by different SASPs across various endospore-forming bacteria. Moreover, it may help uncover the molecular mechanisms by which germination factors destabilize SASP-DNA interactions and regulate gene expression during the transition from dormancy to the vegetative state.

#### Methods

#### Purification of Ssp4 variants

The pET-28b encoding  $\mathrm{Ssp4}_{\mathrm{G36}}$  was obtained by commercial gene synthesis (BIONICS), and  $\mathrm{Ssp4}_{\mathrm{D36}}$  (pYK076) was generated by substituting glycine with aspartic acid at residue 36. These plasmids produce His-tagged Ssp4 with a thrombin protease cleavage site. Each Ssp4 plasmid was transformed into BL21(DE3) cells and then grown in 30 mL LB with 50 µg/mL kanamycin at 37 °C. The pre-culture was diluted at a 1:100 ratio into 1.8 L LB with vigorous shaking until OD<sub>600</sub> reached ~ 0.5, then 0.4 mM IPTG was added and incubated for 4 h at 37 °C. The cells were harvested and resuspended in 45 mL lysis buffer (20 mM Tris-HCl pH 8.0, 150 mM NaCl, 1 mM β-mercaptoethanol (BME), 0.1 mM PMSF, and EDTA-free protease inhibitor cocktail). The cells were lysed by sonication and centrifuged at 40,000×g and 4 °C for 35 min. The supernatant with 30 mM imidazole was loaded on 5 mL HisTrap FF crude column (Cytiva) pre-equilibrated and then washed with Nickel buffer (20 mM Tris-acetate pH 7.3, 500 mM NaCl, 1 mM BME, 10% glycerol (v/v)) containing 30 mM Imidazole. The His-tagged Ssp4 was eluted with 18 CV linear gradient of 30-300 mM imidazole with the Nickel buffer, and peak fractions were analyzed by 15% SDS-PAGE. The fractions containing Ssp4 were collected and concentrated with a centrifugal filter (Amicon Ultra 10 K) until the sample volume reached ~ 600 µl. Next, the sample was loaded onto a HiLoad 16/600 Superdex 200 pg column pre-equilibrated with Superdex 200 buffer (20 mM Tris-acetate pH 7.3, 100 mM NaCl, 1 mM BME, 10% glycerol (v/v)). Our purified protein had an average 260/280 ratio of 0.55, falling within the high purity range. The peak fractions were confirmed by 15% SDS-PAGE, and the protein fractions were combined. The protein aliquots were flash-frozen in liquid nitrogen and stored at -80 °C.

To remove the His-tag, we reconstructed the plasmids to encode His-tagged Ssp4 with a TEV protease cleavage site, replacing the original thrombin site. Eluted fractions from the HisTrap FF crude column containing His-tagged Ss4 were subjected to TEV protease cleavage in TEV buffer (50 mM Tris-HCl pH 7.5, 100 mM NaCl, 1 mM DTT) by dialysis using 7000 MWCO SnakeSkin Dialysis Tubing (Thermo Fisher) at 4 °C. Following TEV cleavage, batch purification using Ni-NTA agarose resin (Qiagen) was performed to remove the cleaved His-tag and His-tagged TEV protease. The sample was then buffer-exchanged into storage buffer (50 mM Tris-HCl pH 7.5, 100 mM NaCl, 1 mM DTT) using a HiPrep desalting column (Cytiva). Verified fractions were combined and flash-frozen for long-term storage at  $-80\,^{\circ}\text{C}$ .

The NMR protein samples were produced with the same purification steps except for main culture medium used for isotope labeling. The isotopically enriched proteins were purified using M9 mineral medium (1x M9 salt solution, 0.4% glucose, 1mM MgSO<sub>4</sub>, 0.3mM CaCl<sub>2</sub>, 1ug/ml Biotin, 1ug/ml Thiamin, 1x trace element solution) instead of LB broth. For 1 L culture, 10 ml of pre-culture grown on LB broth was centrifuged at 6000×g for 15 min to remove LB and resuspended with M9 mineral medium containing 50 µg/mL kanamycin. To make isotope-labeled protein, 0.5 g of  $^{15}$ N-NH<sub>4</sub>Cl (Cambridge Isotope Laboratories, NLM-467-5) or 3 g of  $^{13}$ C-glucose (Cambridge Isotope Laboratories, CLM-1396-5) was added to 1 L of M9 mineral medium. When the culture were grown until OD<sub>600</sub> reached ~ 0.6, 0.4mM IPTG was added and incubated at 37 °C for 4 h.

#### Electrophoretic mobility shift assay (EMSA)

The various sizes of double-strand DNA (dsDNA) were obtained by PCR and purified using a gel extraction kit (Qiagen). The DNA binding reactions for Ssp4 were performed in the reaction buffer (20 mM Tris-acetate pH 7.3, 100 mM NaCl, 10% glycerol (v/v)) at a total volume of 25  $\mu$ l containing 20 nM DNA with 0.05, 0.1, 0.3, 0.5, 0.9, 2.4, 5.6, or 10  $\mu$ M Ssp4. Each sample was mixed thoroughly and incubated at room temperature for 15 min. Each reaction sample was loaded onto a 6% native-PAGE gel that was pre-run in 1x TG buffer (25 mM tris, 192 mM glycine) at 80 V for 40 min. The electrophoresis for each sample was conducted in 1x TG buffer at 60 V for at least 2 h in cold water. The gel was stained for 30 min in 100 mL 1x TAE (Tris-acetate-EDTA) containing 5  $\mu$ l

SYBR Green I Nucleic Acid Gel Stain (Invitrogen). The DNA was visualized under UV light using a gel imaging system. The intensity of each DNA band was quantified using ImageJ software, and the Ssp4-bound DNA fraction was calculated by comparing it with the free DNA intensity. The data were fit to a Hill slope equation by GraphPad Prism software, and the half-maximal concentration constant  $(K_{0.5})$  and Hill slope (h) were obtained. The curves were obtained by fitting the percentage of DNA bound to the Hill equation:

$$y = \frac{B_{max}x^{h}}{K_{0.5}^{h} + x^{h}}$$

The fitted curves on the logarithmic X-axis are according to the sigmoidal shape saturated in 100%.

#### **DNA** protection assay

To test the ability of DNA protection against UV, 20 nM of 300 bp DNA was used in the reaction buffer. To damage the DNA, 365 nm UV-A applying 12 mW instant power was irradiated on the sample for 20, 40, and 60 min, and then 2% SDS (w/v) with loading dye (NEB #B7024S) was added to stop the reaction. The entire volume of samples was loaded on 6% native-PAGE gel pre-run at 80 V and the electrophoresis was conducted at 60 V in 1x TG buffer. The gel was imaged under UV light after staining for 30 min in 1x TAE buffer containing SYBR Green I Nucleic Acid Gel Stain. To analyze the degree of UV protection by Ssp4, DNA was incubated with 0.9  $\mu$ M Ssp4 in a 13  $\mu$ l reaction mixture to allow binding, followed by UV irradiation for 10–20 min. To exclude the band shift on gel due to Ssp4 binding, 2% SDS (w/v) was added and loaded on 6% native-PAGE gel. The gel was visualized in the same condition as the above UV-A effect test, except the gel was run initially at 60 V and then increased to 100 V. The degree of band shift was analyzed using ImageJ software.

For nuclease digestion, DNase I was treated on Ssp4-bound DNA. 20 nM 300 bp DNA was assembled with 0.3, 0.5, 0.9, or 2.4  $\mu$ M Ssp4 in 10  $\mu$ l reaction and then incubated for 15 min at room temperature. The DNase I (Enzynomcis) diluted to 1 unit/ $\mu$ l in dilution buffer (25 mM Tris-HCl pH 7.6, 50% glycerol (v/v)) was added in the samples with DNase I buffer to consist of 40 mM Tris-acetate pH 7.3, 10 mM NaCl, 6 mM MgCl, 1 mM CaCl,. These reactions were incubated for 30 min at room temperature. To disassociate the Ssp4 from DNA and inactive the DNase I, 2% SDS (w/v) and 8 mM EDTA was added to the sample with loading dye (NEB #B7024S) and then incubated for 10 min at room temperature. The entire volume of each sample was loaded on 6% native-PAGE gel pre-run at 80 V. The electrophoresis was conducted at 60 V for 40 min and then continued for about 80 min at 100 V in the cold water. The staining was performed by 5  $\mu$ l SYBR Green I Nucleic Acid Gel Stain in 100 ml 1x TAE buffer for 30 min. The bands detected by a UV-based gel imaging system were analyzed using ImageJ software.

#### Purification of sortase A

The pet30b-7 M SrtA (Addgene plasmid #51141) was thankfully gifted from Hidde Ploegh. The plasmid was transformed into BL21(DE3) cells, and a select transformant with appropriate antibiotics was used to overexpress the protein. When 1.8 L LB culture was grown until OD<sub>600</sub> reached ~ 0.6, the sortase A was induced by adding 0.5 mM IPTG and continued the growth overnight at 25 °C. The cells were harvested by centrifugation and resuspended in 45 mL lysis buffer (50 mM Tris-HCl pH 7.5, 150 mM NaCl, 10 mM Imidazole, 10% glycerol (v/v), 1x cOmplete™ Protease Inhibitor cocktail, 1 mM PMSF). The cells were lysed by sonication on ice, and the lysate was centrifuged at 35,000×g for 45 min at 4 °C. The supernatant was passed through the 1.5 mL Ni-NTA agarose resin (Qiagen) in a glass gravity column (Bio-rad) and washed with Sortase wash buffer (50 mM Tris-HCl pH 7.5, 150 mM NaCl, 10 mM imidazole, 10% glycerol (v/v)). The protein was eluted in 1 mL fractions with Sortase elution buffer (50 mM Tris-HCl pH 7.5, 150 mM NaCl, 300 mM imidazole, 10% glycerol (v/v)) until there was no detection by Bradford assay. The fractions were analyzed using 15% SDS-PAGE, and the fractions containing sortase A were pooled. Dialysis was performed against Sortase dialysis buffer (50 mM Tris-HCl pH 8.0, 150 mM NaCl) using 7000 MWCO SnakeSkin Dialysis Tubing (Thermo Fisher). The dialyzed sample was concentrated using a centrifugal filter (Amicon Ultra 10 K Centrifugal Filter Unit, Millipore) at 4 °C, and glycerol was added for a final concentration of 10%. The sample was aliquoted, flash-frozen in liquid nitrogen, and stored at -80 °C.

#### Fluorescent labeling of Ssp4 by sortase A

For the sortase-mediated fluorescent labeling, we inserted N-terminal GGG residues for the Ssp4 plasmids by site-directed mutagenesis and replaced a preexisting thrombin site with a TEV cleavage site<sup>28</sup>. The sequence-confirmed construct was amplified and stored at -20 °C (pYK078 and pYK082 for Ssp4 $_{G36}$  and Ssp4 $_{D36}$  respectively). To obtain fluorescently labeled Ssp4, the N-terminal domain containing a 6xHis-tag was removed by TEV protease, and the serial glycine residues were exposed. Subsequently, a labeling reaction with atto488-conjugated LPETGG was conducted by sortase A, and then the labeled proteins were purified by nickel-charged resin reaction followed by dialysis to remove the enzymes and free GG fragments in the sample.

#### TIRF microscope and flowcell

Flowcells used for single-molecule assay were prepared as previously described<sup>26</sup>. Briefly, the flowcell surface was passivated by a supported lipid bilayer, and 0.1 mg/mL streptavidin was incubated to coat the surface in BSA buffer (40 mM Tris pH 8.0, 1 mM MgCl<sub>2</sub>, 0.2 mg/mL BSA, 50 mM NaCl, 1 mM DTT). This allowed the biotinylated  $\lambda$ -DNA to immobilize on the surface via biotin-streptavidin interaction, and buffer flow was manipulated with an electric syringe pump (Chemyx, Fusin 200-X). DNA was stretched and visualized at 0.4 mL/min flow rate in the imaging buffer (40 mM Tris pH 7.3, 1 mM MgCl<sub>2</sub>, 0.2 mg/mL BSA, 1 mM DTT,  $\pm$ 

100 nM DPA with  $CaCl_2$ ) and  $\sim$  30 nM Ssp4 protein was introduced into the flowcell to observe its dynamic association on DNA.

#### Single-molecule imaging & analysis

Single-molecule images were collected in Nikon Ti-2 microscope equipped with 60x water immersion objective lens (Nikon, VC 60XC WI) and a customized prism-TIRF configuration at 1s intervals with 200ms exposure time in NIS-Elements software (Nikon). Flowcells were illuminated by a 50 mW 488 nm laser light (Cobolt) through a quartz prism. The fluorescence signal from the flowcell was selected by a dichroic filter (Chroma, T635lpxr) with an emission filter (Chroma, AT495lp) and recorded with an EMCCD (Teledyne Photometrics, Evolve 16) camera. Images were saved as TIFF files without compression, and further analysis was done in Image J (NIH), MATLAB (Mathworks), and OriginPro.

To measure the difference of binding affinity of each Ssp4 variant on DNA, a minimum of three tiff frames were combined using the 'Image Calculator', starting from the brightest regions in the tiff stack in ImageJ. We selected individual DNA molecules and normalized the fluorescence intensity at each position along the  $\lambda$ -DNA where Ssp4 bound the DNA. Next, we calculated the average normalized intensity using the normalized intensity from all individual DNA molecules in MATLAB scripts. Then, we plotted a scatter plot between Ssp4 $_{\rm G36}$  and Ssp4 $_{\rm D36}$  normalized intensity to measure the correlation between two Ssp4 variants in OriginPro. To obtain the half-life, the fluorescence intensity of Ssp4-Atto488 was calculated by summing the intensities of all pixels between the ends of the DNA in each frame, excluding the barrier in MATLAB scripts. The total intensities of each frame were normalized and fitted to a single exponential decay (  $y=y_0+A_1e^{-x^2t_1}$ ) and half-life (  $t^{1/2}=t_1*In(2)$ ) was obtained.

#### NMR spectroscopy

For NMR experiments, we used an Avance III HD 850 MHz NMR spectrometer equipped with a cryogenic HCN probe (Bruker, Billerica, MA, USA). All the NMR samples were prepared to 300 µl for accommodation into a 5-mm Shigemi tube (Sigma-Aldrich). The sample temperature was maintained at 288 K, unless stated otherwise. For NMR data acquisition, the TopSpin 3.2 software package (Bruker) was used and the POKY software suite was employed for subsequent signal assignment and data analysis<sup>35</sup>.

The chemical shift assignment of Ssp4 was conducted by collecting the following NMR spectra:  $2D^{-1.5}N$  heteronuclear single-quantum coherence (HSQC), 3D HNCO, 3D HN(CA)CO, 3D HNCA, 3D HN(CO)CA, and 3D HNCACB. The sample contained 400  $\mu$ M of a uniformly  $^{13}C$ - and  $^{15}N$ -labeled ([ $U^{-13}C$ ;  $U^{-15}N$ ]) Ssp4 $_{D36}$  sample along with the buffer consisting of 20 mM Tris-acetate pH 7.3, 100 mM NaCl, 1 mM BME, 10% glycerol (v/v), 0.5 mM sodium trimethylsilylpropanesulfonate (DSS), and 7%  $D_2O$  (v/v). The signal from DSS was used for NMR spectral referencing. The resonance assignment results were deposited to the Biological Magnetic Resonance Data Bank with the accession number 52,437. The chemical shift data was extracted with the format conversion tool in POKY, and it was subsequently analyzed by TALOS-N for secondary structure prediction  $^{36,46}$ .

The titration experiments with duplex DNA were conducted by serially adding DNA (dissolved in the same buffer of the NMR sample) to the 100  $\mu$ M [U- $^{15}$ N]-Ssp4 $_{D36}$  sample and collecting 2D  $^{1}H$ - $^{15}$ N HSQC spectra. Two DNA duplexes were employed for the titration: 5'-ATCTATTTTTGTTATAACGTTTGGCTTAGA-3' (AT-rich DNA) and 5'-GTCCGCGCGGGCTTCGCTC-3' (GC-rich DNA). The chemical shift perturbation (CSP) upon DNA addition was plotted by calculating  $\Delta\delta_{NH}$  for each signal:  $\Delta\delta_{NH}=[(\Delta\delta_{N}/5)^2+(\Delta\delta_{H})^2]^{1/2}$ , where  $\Delta\delta_{N}$  and  $\Delta\delta_{H}$  are the signal shifts (in ppm) in the NMR spectra of DNA-free and bound Ssp4 $_{D36}$ . In addition, we repeated the similar experiments for Ssp4 $_{G36}$ . The NMR signals of [U- $^{15}$ N]-Ssp4 $_{G36}$  were assigned based on their spectral similarity with those of Ssp4 $_{D36}$ . Subsequently, we conducted the titration experiments; the GC-rich duplex DNA was serially added to the 100  $\mu$ M [U- $^{15}$ N]-Ssp4 $_{G36}$  sample, and 2D  $^{1}$ - $^{15}$  N HSQC spectra were collected. The CSP results for Ssp4 $_{G36}$  were analyzed using the same procedure as those for Ssp4 $_{D36}$ .

#### CD (circular dichroism) spectrometry

The DNA sample was prepared in 20mM Tris-HCl (pH 7.3) and 100mM NaCl, with a DNA concentration of 10  $\mu$ M. The DNA used was prepared as a duplex, and its sequence was 5'-ATATATACATCCTGTTCCAATGTGATCAGCTGCACCCCATGAGGGTGGGGAGGGTGGGGAAAAGTGTGATCAGCTGCTCGGGCATGTATTGAACAG-3'. DPA (2,6-Pyridinedicarboxylic acid, Sigma) was filtered using a 0.22  $\mu$ m filter before preparing the stock solution. Calcium chloride dihydrate (Sigma) was used to prepare the Ca²+ stock solution, and the two solutions were mixed at a 1:1 ratio and incubated at room temperature for 20 min to generate DPA-Ca²+. This prepared DPA-Ca²+ solution was added to the DNA sample to reach a final concentration of 10  $\mu$ M. Circular Dichroism (CD) spectrometry was performed using a J-1500 CD spectrometer (JASCO, KBSI) at 25 °C with a 1 mm path length cell and a sample volume of 200  $\mu$ L, and the spectral measurements were detected across a wavelength range of 200–300 nm. The resulting CD data were fitted using Origin software to analyze potential changes in DNA secondary structure.

#### Statistics and reproducibility

The EMSA data were reported as a mean ± standard error of the mean (S.E.M), and unpaired t-tests were performed for statistical group comparisons using GraphPad Prism software. In the DNase I assay, we normalized the degree of degradation by setting the value of the intact DNA to 1.0. One-way analysis of variance (ANOVA) was conducted using GraphPad Prism to determine the significance of Ssp4 on protecting DNA against DNase I. The four asterisks indicate *P*-values less than or equal to 0.0001. ns shows not significant differences between Ssp4 concentrations.

We used a two-sample t-test to compare the half-lives between conditions using OriginPro. The significance threshold was set at 0.05 in all tests.

#### Software and tools

The following software tools were used during data analysis, figure preparation, and structural modeling in this study. Affinity designer 2 (v2.6.3; Serif, https://affinity.serif.com/designer/) was used for figure consistency and clarity. TopSpin 3.2 (Bruker, https://www.bruker.com/) was used for NMR data acquisition and processing. POKY (developed by Woonghee Lee, University of Colorado-Denver; https://sites.google.com/view/pokynmr/home) was used for NMR data analysis. TALOS-N (v4.21; NIH, https://spin.niddk.nih.gov/bax/software/TALOS-N) was employed for secondary structure prediction from NMR data. ImageJ (v1.53e; NIH, https://imagej.net/ij/) was used to process gel electrophoresis images. OriginPro 2021 (OriginLab, https://www.originlab.com/2021) was used for figure generation. MATLAB (R2023a; MathWorks, https://www.mathworks.com/) was used for the analysis of single-molecule data. AlphaFold Server (AlphaFold 3; https://alphafoldserver.com) was used to predict protein structures and their interactions with DNA. PyMOL (v3.1.6.1; Schrödinger, https://pymol.org/) was used to visualize and refine predicted protein structures. GraphPad Prism (v9; GraphPad, https://www.graphpad.com/) was used to generate graphs and perform curve fitting. NIS-Elements AR (v5.30.01; Nikon, https://www.microscope.healthcare.nikon.com/) was used for time-lapse TIRF microscopy imaging and recording.

#### Data availability

The resonance assignment data is available in the Biological Magnetic Resonance Data Bank under accession number 52,437 (direct link: https://bmrb.io/author\_view/52437\_hy\_mmrlmrdv.str). All other data are available in the manuscript and supplementary information.

Received: 24 April 2025; Accepted: 19 September 2025

Published online: 24 October 2025

#### References

- 1. Mehdizadeh Gohari, I. et al. Pathogenicity and virulence of Clostridium perfringens. Virulence 12, 723-753 (2021).
- 2. Uzal, F. A. et al. Towards an Understanding of the role of *Clostridium perfringens* toxins in human and animal disease. *Future Microbiol.* 9, 361–377 (2014).
- 3. Li, J., Miyamoto, K., Sayeed, S. & McClane, B. A. Organization of the cpe Locus in CPE-Positive *Clostridium perfringens* Type C and D Isolates. *PLoS One* 5, e10932 (2010).
- 4. Shrestha, A., Uzal, F. A. & McClane, B. A. Enterotoxic clostridia: Clostridium perfringens enteric diseases. Microbiol. Spectr. 6, (2018).
- 5. Nicholson, W. L., Munakata, N., Horneck, G., Melosh, H. J. & Setlow, P. Resistance of *Bacillus* endospores to extreme terrestrial and extraterrestrial environments. *Microbiol. Mol. Biol. Rev.* 64, 548–572 (2000).
- 6. Setlow, P. Spore resistance properties. Microbiol. Spectr. 2, (2014).
- 7. Driks, A. Maximum shields: the assembly and function of the bacterial spore coat. Trends Microbiol. 10, 251-254 (2002).
- 8. Setlow, P. I will survive: DNA protection in bacterial spores. Trends Microbiol. 15, 172-180 (2007).
- 9. Setlow, P. Spores of *Bacillus subtilis*: their resistance to and killing by radiation, heat and chemicals. *J. Appl. Microbiol.* **101**, 514–525 (2006).
- 10. Magge, A. et al. Role of dipicolinic acid in the germination, stability, and viability of spores of *Bacillus subtilis. J. Bacteriol.* **190**, 4798–4807 (2008).
- 11. Raju, D., Waters, M., Setlow, P. & Sarker, M. R. Investigating the role of small, acid-soluble spore proteins (SASPs) in the resistance of *Clostridium perfringens* spores to heat. *BMC Microbiol.* **6**, 50 (2006).
- Cowan, A. E., Koppel, D. E., Setlow, B. & Setlow, P. A soluble protein is immobile in dormant spores of *Bacillus subtilis* but is mobile in germinated spores: implications for spore dormancy. *Proc. Natl. Acad. Sci. U S A.* 100, 4209–4214 (2003).
  Paredes Sabia D. Paiu D. Torres I. A. & Sarker M. P. Pole of small acid soluble spore proteins in the resistance of *Clastridium*.
- 13. Paredes-Sabja, D., Raju, D., Torres, J. A. & Sarker, M. R. Role of small, acid-soluble spore proteins in the resistance of *Clostridium perfringens* spores to chemicals. *Int. J. Food Microbiol.* **122**, 333–335 (2008).
- 14. Meaney, C. A., Cartman, S. T., McClure, P. J. & Minton, N. P. The role of small acid-soluble proteins (SASPs) in protection of spores of *Clostridium botulinum* against nitrous acid. *Int. J. Food Microbiol.* **216**, 25–30 (2016).
- Raju, D., Setlow, P. & Sarker, M. R. Antisense-RNA-Mediated decreased synthesis of Small, Acid-Soluble spore proteins leads to decreased resistance of *Clostridium perfringens* spores to moist heat and UV radiation. *Appl. Environ. Microbiol.* 73, 2048–2053 (2007).
- Li, J. & McClane, B. A. A novel small acid soluble protein variant is important for spore resistance of most Clostridium perfringens food poisoning isolates. PLoS Pathog. 4, e1000056 (2008).
- 17. Li, J., Paredes-Sabja, D., Sarker, M. R. & McClane, B. A. Further characterization of *Clostridium perfringens* small acid soluble protein-4 (Ssp4) properties and expression. *PLoS One.* 4, e6249 (2009).
- 18. Setlow, B. & Setlow, P. Binding of small, acid-soluble spore proteins to DNA plays a significant role in the resistance of *Bacillus subtilis* spores to hydrogen peroxide. *Appl. Environ. Microbiol.* **59**, 3418–3423 (1993).
- Fairhead, H. & Setlow, P. Binding of DNA to alpha/beta-type small, acid-soluble proteins from spores of *Bacillus* or *Clostridium* species prevents formation of cytosine dimers, cytosine-thymine dimers, and bipyrimidine photoadducts after UV irradiation. *J. Bacteriol.* 174, 2874–2880 (1992).
- Setlow, B., Sun, D. & Setlow, P. Interaction between DNA and alpha/beta-type small, acid-soluble spore proteins: a new class of DNA-binding protein. J. Bacteriol. 174, 2312–2322 (1992).
- Lee, J. H., Voo, K. S. & Skalnik, D. G. Identification and characterization of the DNA binding domain of CpG-binding protein. J. Biol. Chem. 276, 44669–44676 (2001).
- Liyanage, R., Krylova, S. M. & Krylov, S. N. Minimizing adsorption of histidine-tagged proteins for the study of protein-deoxyribonucleic acid interactions by kinetic capillary electrophoresis. J. Chromatogr. A. 1322, 90–96 (2013).
- 23. Lysetska, M. et al. UV light-damaged DNA and its interaction with human replication protein A: an atomic force microscopy study. *Nucleic Acids Res.* **30**, 2686–2691 (2002).
- Nicholson, W. L., Setlow, B. & Setlow, P. Ultraviolet irradiation of DNA complexed with alpha/beta-type small, acid-soluble proteins from spores of *Bacillus* or *Clostridium* species makes spore photoproduct but not thymine dimers. *Proc. Natl. Acad. Sci. U S A.* 88, 8288–8292 (1991).
- Douki, T., Setlow, B. & Setlow, P. Photosensitization of DNA by dipicolinic acid, a major component of spores of Bacillus species. Photochem. Photobiol Sci. 4, 591–597 (2005).
- Soniat, M. M. et al. Next-Generation DNA curtains for Single-Molecule studies of homologous recombination. *Meth Enzymol.* 592, 259–281 (2017).
- Heo, W., Seo, J., Lee, Y. & Kim, Y. Fluid-driven DNA stretching for single-molecule studies on chromatin-associated proteins. Biochem. Biophys. Res. Commun. 634, 122–128 (2022).

- 28. Sarpong, K. & Bose, R. Efficient sortase-mediated N-terminal labeling of TEV protease cleaved Recombinant proteins. *Anal. Biochem.* **521**, 55–58 (2017).
- Shimizu, T. et al. Complete genome sequence of Clostridium perfringens, an anaerobic flesh-eater. Proc. Natl. Acad. Sci. U S A. 99, 996–1001 (2002).
- 30. Jamroskovic, J. et al. Variability in DPA and calcium content in the spores of Clostridium species. Front. Microbiol. 7, 1791 (2016).
- 31. Hintze, P. E. & Nicholson, W. L. Single-spore elemental analyses indicate that dipicolinic acid-deficient *Bacillus subtilis* spores fail to accumulate calcium. *Arch. Microbiol.* **192**, 493–497 (2010).
- 32. Gao, Y. et al. The SpoVA membrane complex is required for dipicolinic acid import during sporulation and export during germination. *Genes Dev.* **36**, 634–646 (2022).
- 33. Varadi, M. et al. AlphaFold protein structure database: massively expanding the structural coverage of protein-sequence space with high-accuracy models. *Nucleic Acids Res.* **50**, D439–D444 (2022).
- 34. Lee, K. S., Bumbaca, D., Kosman, J., Setlow, P. & Jedrzejas, M. J. Structure of a protein-DNA complex essential for DNA protection in spores of *Bacillus* species. *Proc. Natl. Acad. Sci. U S A.* 105, 2806–2811 (2008).
- 35. Lee, W., Rahimi, M., Lee, Y. & Chiu, A. POKY: a software suite for multidimensional NMR and 3D structure calculation of biomolecules. *Bioinformatics* 37, 3041–3042 (2021).
- Shen, Y. & Bax, A. Protein backbone and sidechain torsion angles predicted from NMR chemical shifts using artificial neural networks. I. Biomol. NMR. 56, 227–241 (2013).
- 37. Setlow, P. DNA in dormant spores of Bacillus species is in an A-like conformation. Mol. Microbiol. 6, 563–567 (1992).
- 38. Setlow, P. Resistance of spores of Bacillus species to ultraviolet light. Environ. Mol. Mutagen. 38, 97-104 (2001).
- 39. Berteau, O. & Benjdia, A. DNA repair by the radical SAM enzyme spore photoproduct lyase: from biochemistry to structural investigations. *Photochem. Photobiol.* **93**, 67–77 (2017).
- 40. Paidhungat, M., Setlow, B., Driks, A. & Setlow, P. Characterization of spores of *Bacillus subtilis* which lack dipicolinic acid. *J. Bacteriol.* **182**, 5505–5512 (2000).
- 41. Kypr, J., Kejnovská, I., Renciuk, D. & Vorlícková, M. Circular dichroism and conformational polymorphism of DNA. *Nucleic Acids Res.* 37, 1713–1725 (2009).
- 42. Ng, H. L. & Dickerson, R. E. Mediation of the A/B-DNA helix transition by G-tracts in the crystal structure of duplex CATGGGCCCATG. *Nucleic Acids Res.* 30, 4061–4067 (2002).
- Xue, J., Wang, P., Li, X., Tan, R. & Zong, W. Transformation characteristics of A-DNA in salt solution revealed through molecular dynamics simulations. *Biophys. Chem.* 288, 106845 (2022).
- 44. Setlow, P. Mechanisms for the prevention of damage to DNA in spores of *Bacillus* species. *Annu. Rev. Microbiol.* 49, 29–54 (1995).
- 45. Nerber, H. N. & Sorg, J. A. The small acid-soluble proteins of *Clostridioides difficile* are important for UV resistance and serve as a check point for sporulation. *PLoS Pathog.* 17, e1009516 (2021).
- 46. Lee, W. et al. PACSY, a relational database management system for protein structure and chemical shift analysis. *J. Biomol. NMR*. 54, 169–179 (2012).
- 47. Deguchi, A. et al. Genetic characterization of type A enterotoxigenic Clostridium perfringens strains. PLoS One. 4, e5598 (2009).
- 48. Li, J. & McClane, B. A. NanH Is produced by sporulating cultures of *Clostridium perfringens* Type F food poisoning strains and enhances the cytotoxicity of *C. perfringens* Enterotoxin. *mSphere* 6, e00176-21 (2021).

#### Acknowledgements

We thank Dr. Young-Sam Lee and Dr. Jeong-Mo Choi for helpful discussions.

#### **Author contributions**

M.K. and H.S. designed and performed gel-based assays, protein purification, and fluorescent labeling. B.K., Y.H.K., and J.H.K. performed NMR data acquisition and analyses. J.K. performed single-molecule assays and analyzed the data. J.B. and Y.K. provided funding and resources. Y.K. supervised the project. All authors contributed to the writing of the manuscript.

#### Funding

This work was supported by the National Research Foundation of Korea [2022R1C1C1005378 to Y.K., RS-2023-00218927 to J.L., 2020R1I1A2074335 to J.H.K.] and by the Institute for Basic Science, Republic of Korea [IBS-R014-A1 to Y.H.K.].

#### **Declarations**

#### Competing interests

The authors declare no competing interests.

#### Additional information

**Supplementary Information** The online version contains supplementary material available at https://doi.org/1 0.1038/s41598-025-21159-3.

Correspondence and requests for materials should be addressed to Y.K.

Reprints and permissions information is available at www.nature.com/reprints.

**Publisher's note** Springer Nature remains neutral with regard to jurisdictional claims in published maps and institutional affiliations.

Open Access This article is licensed under a Creative Commons Attribution-NonCommercial-NoDerivatives 4.0 International License, which permits any non-commercial use, sharing, distribution and reproduction in any medium or format, as long as you give appropriate credit to the original author(s) and the source, provide a link to the Creative Commons licence, and indicate if you modified the licensed material. You do not have permission under this licence to share adapted material derived from this article or parts of it. The images or other third party material in this article are included in the article's Creative Commons licence, unless indicated otherwise in a credit line to the material. If material is not included in the article's Creative Commons licence and your intended use is not permitted by statutory regulation or exceeds the permitted use, you will need to obtain permission directly from the copyright holder. To view a copy of this licence, visit <a href="http://creativecommons.org/licenses/by-nc-nd/4.0/">http://creativecommons.org/licenses/by-nc-nd/4.0/</a>.

© The Author(s) 2025